Article

A Nonlinear Observer for Remotely Operated Vehicles with Cable Effect in Ocean Currents

Xiang Li, Min Zhao * and Tong Ge

State Key Laboratory of Ocean Engineering, Collaborative Innovation Center for Advanced Ship and Deep-Sea Exploration, Shanghai Jiao Tong University, Shanghai 200240, China; lixiang.sjtu@hotmail.com (X.L.); tongge@sjtu.edu.cn (T.G.)

* Correspondence: min.zhao@sjtu.edu.cn; Tel.: +86-021-3420-8063

check for updates

Featured Application: Applying on Observer and Controller for Remotely Operated Vehicles.

Abstract: A nonlinear observer for a remotely operated vehicle (ROV) is investigated, and a four-degree-of-freedom nonlinear sliding state observer is designed in this study. An ocean current model and a simplified umbilical cable disturbing force model of ROVs were set up; the simplified cable force model characterized the cable disturbing force. The velocity information and the cable force were observed and estimated both online and in real time. We proved that the observation error was uniformly ultimately bounded. The modeling of the disturbing force and the compensation for the observer was an effective method to improve the observation precision and to reduce the chattering of the observer outputs.

---

1. Introduction

The improvement of marine resources exploitation technology has become important for the development of the marine industry. The design and development of new types of marine engineering equipment to enhance the technological level of the ocean engineering industry is of considerable significance. Because of the complexity of the marine environment, underwater vehicles have become an important and valuable tool for the exploration and development of marine resources. Unmanned underwater vehicles, including remotely operated vehicles (ROVs), autonomous underwater vehicles (AUVs), and underwater gliders, have been extensively and increasingly used in marine environments for exploration, inspection, and engineering operations [1]. They can provide safe and effective access to deep sea and hadal environments without physically entering them.

With advantages like functional diversity, strong operational ability, and a high safety factor, ROVs have been widely used and have become important technical equipment in areas such as ocean resource development, exploration, marine scientific research, and underwater engineering [2].

To guarantee the operation quality, high precision, and safety of ROVs, a high-performance controller for the trajectory tracking or station-keeping of ROVs is required. In practice, there are a number of technical challenges in the control of an underwater vehicle, such as model uncertainties and unknown external disturbances [3–7]. The model uncertainties of ROVs are usually caused by inaccurate hydrodynamic coefficients, which are obtained using towing tank experiments or computational fluid dynamics methods. The unknown disturbances in practical oceanic environments often include currents, waves, and tides. For the control design of ROVs, the external disturbing force caused by the cable that connects with the support ship should also be considered. The currents

and the umbilical cable simultaneously affect the ROV motions as the umbilical cable is connected to the ROV.

In many works on the control of underwater dynamic systems, the state vector is assumed to be measured. The quality of feedback signals from the ROV sensor system plays an important role in the control performance of the vehicle as the signals affected by noises can debase the control quality and even lead to system instability [8]. However, in practice, it is difficult or impossible to measure all of the state variables of an ROV system with sensors for technical or economic reasons. For example, cable disturbing force cannot be easily obtained with normal sensors, and there is not enough money to buy high-precision but expensive sensors. Hence, effective state observers for ROVs need to be developed to provide accurate and robust signals. Moreover, it is necessary and is of considerable significance to design an observer to fully know the state variables of the system. The state observers for vehicles have been studied by a number of researchers in the past [9–12]. The use of a complementary observer is one of the most popular techniques for sensor combination. The algorithm allows for straightforward implementation without requiring high computational resources and is suitable for small and low-cost autonomous vehicles with limited onboard power. The linear observer has been solved by Kalman and Luenberger, but the nonlinear case is still an active domain of research. Gauthier et al. developed the high-gain observer approach, which is closely related to the triangular structure and is derived from the uniform observability of nonlinear systems [13]. Fridman et al. proposed a higher-order sliding-mode observer to estimate precisely the observable states and asymptotically the unobservable ones in a multi-input-multi-output nonlinear system with unknown inputs and stable internal dynamics [14]. Rezazadegan and Chatraei derived an adaptive control law for a six-degree-of-freedom (6-DOF) model for the trajectory tracking problem of an underactuated underwater vehicle in the presence of a parametric uncertainty [15]. Khadhraoui et al. proposed to control ROVs for exploration in sub-sea historical sites and designed a nonlinear observer to estimate the linear and angular velocity of an ROV [16]. Chu et al. developed a new adaptive neural network control approach for a class of ROVs and introduced an adaptive observer for the velocity state and angular velocity state estimation with a local recurrent neural network [17].

In complex missions, an ROV often requires a high degree of autonomy, precision, and maneuverability. Moreover, a single sensor is not sufficient to obtain the position and velocity information of the ROV because each type of sensor has its own disadvantages. Thus, ROVs are usually equipped with different types of sensors, such as the inertial measurement unit (IMU) and the velocity log [18]. The IMU can measure the linear accelerations and the rotational velocity of the vehicle. Further, the velocity log, usually a Doppler velocity log (DVL), can measure the linear velocities of the vehicle. The IMU and the DVL measurements are usually combined to provide stable linear velocity, angular velocity, and orientation signals. Depending on the quality of the onboard IMU, the position of the vehicle can be computed from the linear acceleration and velocity measurements. However, because of the inevitable drift in the IMU and DVL, the position estimate will not be stable over time. When the ROV swims through the water, ocean currents always have an influence on the motion of the ROV. To increase the performance, accuracy, and the situation awareness of the ROV, the estimation of the ocean current velocity is often desired. However, the IMU can only measure the total acceleration experienced by the vehicle and cannot distinguish between the motion induced by the ocean current and that induced by the onboard propulsion system. Moreover, the DVL cannot measure the ocean current velocity in its usual configuration. As the hydrodynamic forces acting on the ROV depend on the velocity of the vehicle with respect to the water, but not the total velocity of the vehicle with respect to the fixed coordinate frame, obtaining the ocean current velocity information can considerably improve the performance of the vehicle control system.

For ocean currents, researchers have developed a variety of observers to estimate the current velocity. Refsnes et al. designed an exponentially stable current observer for a reduced-order dynamic vehicle model, and used the estimated current velocity to compute the hydrodynamic forces and moments more accurately for inclusion in a feedback control strategy. Further, the observer only

required position measurements [19]. Aguiar and Pascoal proposed an estimation scheme and designed a kinematic observer for ocean current estimation. The proposed observer provides exponential convergence to the true ocean current velocity, but requires the knowledge of both the position and the relative velocity of the vehicle [20]. Børhaug et al. took a model-based approach and designed a six-degree-of-freedom (6-DOF) observer for the ocean current velocity on the basis of the dynamic model and the measurement of the linear velocity of the vehicle [21].

The deep sea ROV systems typically consist of a large support vessel, a winch, umbilical cable, and ROV. Thus far, most of the research has focused on the numerical simulation and prediction of the cable configuration and the ROV motion with the cable effect [22–24]. However, few studies have dealt with motion control models for ROVs considering the cable disturbing force and the current effects because of the corresponding complexity and difficulty.

As the ocean current velocity and the cable disturbing force cannot be measured by the standard onboard sensors, the development of an estimation scheme is required. In this paper, a nonlinear observer for the state estimation of a tethered ROV system in slowly varying ocean currents is proposed. The observer will estimate the velocity state, the external current velocity, and the cable disturbance.

The rest of this paper is organized as follows. In Section 2, the kinematic and dynamic models of ROVs are introduced and formulated. In Section 3, numerical methods for discrete model solutions are given. In Section 4, a nonlinear observer is proposed for estimating velocities, unknown ocean currents, and the cable disturbing force, and the stability properties of the observer are analyzed. Then, in Section 5, the performance of the proposed observer is illustrated through case studies. Finally, the conclusions are presented in Section 6.

2. ROV Description

The deep sea ROV "Sea Dragon" is a large-scale working class ROV developed and built by the Underwater Engineering Research Institute of Shanghai Jiao Tong University (Figure 1). The results presented in this paper are based on the Sea Dragon ROV. The main physical data of the ROV are reported in Table 1. The ROV is equipped with seven thrusters (three vertical and four horizontal). The position of the thrusters on the vehicle is shown in Figure 2.

Figure 1. The Sea Dragon remotely operated vehicle (ROV) at sea.

Table 1. Main parameters of the ROV.

Parameter	Value
Mass in the air (kg)	3450
Mass in the water (kg)	0
Working depth (m)	3500
Length $\times$ width $\times$ height (m)	$3.17 \times 1.81 \times 1.76$
Coordinate of buoyancy center (m)	0, 0, -0.4
Coordinate of gravity center (m)	0, 0, 0
Moment of inertia I_{xx}, I_{yy}, I_{zz} (kgm^2)	2200, 710, 652
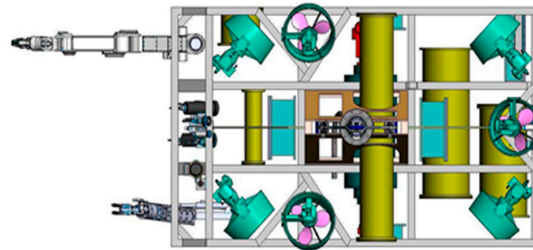
Figure 2. Thruster configuration of ROVs.

The sensor set available for the working class ROV includes:

- The global positioning system (GPS);
- Ultra-short baseline (USBL);
- Altimeter: 200 kHz transmit frequency standard, depth rating 6000 m;
- Depth sensor: 6000 m rating, 0.01% accuracy;
- The inertial measurement unit (IMU);
- Doppler Velocity Log (DVL): working frequency 600 kHz, 0.3% full scale accuracy.

An Ordinary Compact PCI industrial control computer is adopted as the upper computer and PC104 is used for the lower computer.

3. Dynamic Model of ROV

3.1. Coordinate Systems

The dynamic model of an underwater vehicle is established and analyzed in two orthogonal coordinate systems, as shown in Figure 3, namely the earth-fixed frame O-XYZ and the body-fixed frame o-xyz.
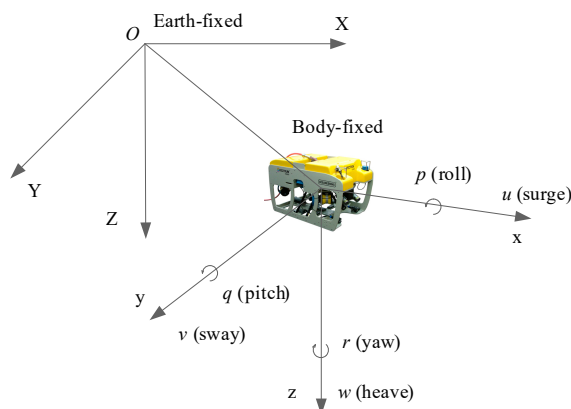
Figure 3. Earth-fixed and body-fixed reference frames.

The earth-fixed frame O-XYZ is a global inertial coordinate system fixed at the ocean surface ship with the origin at O. The OZ axis points vertically down to the water, and the OX and OY axes are in two mutually perpendicular horizontal directions.

The body-fixed frame o-xyz is a local coordinate system fixed on the vehicle with the origin at o. Here, the ox axis points to the front of the vehicle, the oz axis points downward, and the oy axis completes the right-hand system with the other two axes.

Underwater remotely operated vehicles have 6-DOF motions, namely, the surge, sway, heave, roll, pitch, and yaw. Three translation displacements, namely X (surge), Y (sway), and Z (heave), and three Euler angles, namely φ (roll), θ (pitch), and ψ (yaw), represent the position and the attitude of the vehicle with respect to the inertial frame, respectively. The instantaneous velocity and the angular velocity with respect to body-fixed frame are represented by (u, v, w) and (p, q, r), respectively.

The transformation of the forces and motions from the global to the local coordinate system can be fulfilled by using the transformation matrix through the Euler angles $\phi\ \theta\ \psi$. The orientation of the vehicle in the global coordinates can be specified by the vector r_o from O to o.

The position of the vehicle is denoted as $\begin{bmatrix} X & Y & Z \end{bmatrix}^T$ in the inertial coordinates (earth-fixed). Linear velocities $\begin{bmatrix} u & v & w \end{bmatrix}^T$ and angular velocities $\begin{bmatrix} p & q & r \end{bmatrix}^T$ are expressed in the body-fixed coordinates. There exists

$$\begin{bmatrix} \dot{X} & \dot{Y} & \dot{Z} \end{bmatrix}^T = J_1 \begin{bmatrix} u & v & w \end{bmatrix}^T \tag{1}$$

where

$$J_1 = \begin{bmatrix} \cos\theta\cos\psi & \sin\varphi\sin\theta\cos\psi - \cos\varphi\sin\psi & \cos\varphi\sin\theta\cos\psi + \sin\varphi\sin\psi \\ \cos\theta\sin\psi & \sin\varphi\sin\theta\sin\psi + \cos\varphi\cos\psi & \cos\varphi\sin\theta\sin\psi - \sin\varphi\cos\psi \\ -\sin\theta & \sin\varphi\cos\theta & \cos\varphi\cos\theta \end{bmatrix} \tag{2}$$

J_1 is the coordinate transformation matrix from the body-fixed to the earth-fixed frame, $J_1{}^{-1} = J_1{}^T$, and J_1 and $J_1{}^{-1}$ are both units of an orthogonal array.

Similarly, the relationship between the angular velocities and the attitude angles can be obtained as follows:

$$\begin{bmatrix} \dot{\varphi} & \dot{\theta} & \dot{\psi} \end{bmatrix}^T = J_2 \begin{bmatrix} p & q & r \end{bmatrix}^T \tag{3}$$

where

$$J_2 = \begin{bmatrix} 1 & \sin\varphi\tan\theta & \cos\varphi\tan\theta \\ 0 & \cos\varphi & -\sin\varphi \\ 0 & \sin\varphi\sec\theta & \cos\varphi\sec\theta \end{bmatrix} \tag{4}$$

3.2. ROV Dynamic Model

In the 6-DOF motion equations of the ROV, $v_1 = \begin{bmatrix} u & v & w \end{bmatrix}^T$ denotes the ROV's velocity in the body-fixed frame, $v_2 = \begin{bmatrix} p & q & r \end{bmatrix}^T$ represents the angular velocity, and $r_g = \begin{bmatrix} x_g & y_g & z_g \end{bmatrix}^T$ is the coordinate of the center of gravity. The momentum equation and the moment of momentum equation of the ROV are expressed as follows [25]:

$$m\left[\dot{v}_1 + v_2 \times v_1 + \dot{v}_2 \times r_G + v_2 \times (v_2 \times r_G)\right] = F \tag{5}$$

$$I_0\dot{v}_2 + v_2 \times (I_0 v_2) + m r_G \times (\dot{v}_1 + v_2 \times v_1) = M \tag{6}$$

where m denotes the mass and I_0 represents the inertial mass moment matrix of the ROV in the body-fixed frame. F and M denote the forces and the moment acting on the center of the ROV, respectively. The two abovementioned equations can be combined as follows:

$$M_{RB}\dot{x} + C_{RB}(v)x = \tau \tag{7}$$

where $x = \begin{bmatrix} v_1 & v_2 \end{bmatrix}^T$, M_{RB} denotes the general mass matrix, and C_{RB} represents the Coriolis matrix. If $r_g = \begin{bmatrix} 0 & 0 & 0 \end{bmatrix}^T$, then

$$M_{RB} = \begin{bmatrix} m & 0 & 0 & 0 & 0 & 0 \\ 0 & m & 0 & 0 & 0 & 0 \\ 0 & 0 & m & 0 & 0 & 0 \\ 0 & 0 & 0 & I_x & -I_{xy} & -I_{xz} \\ 0 & 0 & 0 & -I_{xy} & I_y & -I_{yz} \\ 0 & 0 & 0 & -I_{xz} & -I_{yz} & I_z \end{bmatrix} \tag{8}$$

$$C_{RB}(x) = \begin{bmatrix} 0 & 0 & 0 & 0 & mw & -mv \\ 0 & 0 & 0 & -mw & 0 & mu \\ 0 & 0 & 0 & mv & -mu & 0 \\ 0 & mw & -mv & 0 & -I_{yz}q - I_{xz}p + I_z r & I_{yz}r + I_{xy}p - I_y q \\ -mw & 0 & mu & I_{yz}q + I_{xz}p - I_z r & 0 & -I_{xz}r - I_{xy}q + I_x p \\ mv & -mu & 0 & -I_{yz}r - I_{xy}p + I_y q & I_{xz}r + I_{xy}q - I_x p & 0 \end{bmatrix} \tag{9}$$

$\tau = \begin{bmatrix} F & M \end{bmatrix}^T$, τ includes all of the external forces, such as gravity, buoyancy, inertia, and viscous forces due to the fluid, propulsion, and the cable tension.

3.3. Added Mass Force on ROV

The added mass force acting on the ROV is defined as follows:

$$F_A = -M_A\dot{x} - C_A(x)x$$

where M_A denotes the general mass matrix and C_A represents the Coriolis matrix corresponding to the added mass of the ROV. M_A and C_A can be further expressed as follows:

$$M_A = -\begin{bmatrix} X_{\dot{u}} & X_{\dot{v}} & X_{\dot{w}} & X_{\dot{p}} & X_{\dot{q}} & X_{\dot{r}} \\ Y_{\dot{u}} & Y_{\dot{v}} & Y_{\dot{w}} & Y_{\dot{p}} & Y_{\dot{q}} & Y_{\dot{r}} \\ Z_{\dot{u}} & Z_{\dot{v}} & Z_{\dot{w}} & Z_{\dot{p}} & Z_{\dot{q}} & Z_{\dot{r}} \\ K_{\dot{u}} & K_{\dot{v}} & K_{\dot{w}} & K_{\dot{p}} & K_{\dot{q}} & K_{\dot{r}} \\ M_{\dot{u}} & M_{\dot{v}} & M_{\dot{w}} & M_{\dot{p}} & M_{\dot{q}} & M_{\dot{r}} \\ N_{\dot{u}} & N_{\dot{v}} & N_{\dot{w}} & N_{\dot{p}} & N_{\dot{q}} & N_{\dot{r}} \end{bmatrix} \tag{10}$$

$$C_A(x) = -\begin{bmatrix} 0 & 0 & 0 & 0 & -a_3 & a_2 \\ 0 & 0 & 0 & a_3 & 0 & -a_1 \\ 0 & 0 & 0 & -a_2 & a_1 & 0 \\ 0 & -a_3 & a_2 & 0 & -b_3 & b_2 \\ a_3 & 0 & -a_1 & b_3 & 0 & -b_1 \\ -a_2 & a_1 & 0 & -b_2 & b_1 & 0 \end{bmatrix} \tag{11}$$

where

$$
\begin{cases}
a_1 = X_{\dot{u}}u + X_{\dot{v}}v + X_{\dot{w}}w + X_{\dot{p}}p + X_{\dot{q}}q + X_{\dot{r}}r \\
a_2 = X_{\dot{v}}u + Y_{\dot{v}}v + Y_{\dot{w}}w + Y_{\dot{p}}p + Y_{\dot{q}}q + Y_{\dot{r}}r \\
a_3 = X_{\dot{w}}u + Y_{\dot{w}}v + Z_{\dot{w}}w + Z_{\dot{p}}p + Z_{\dot{q}}q + Z_{\dot{r}}r \\
b_1 = X_{\dot{p}}u + Y_{\dot{p}}v + Z_{\dot{p}}w + K_{\dot{p}}p + K_{\dot{p}}q + K_{\dot{r}}r \\
b_2 = X_{\dot{q}}u + Y_{\dot{q}}v + Z_{\dot{q}}w + K_{\dot{q}}p + M_{\dot{q}}q + M_{\dot{r}}r \\
b_3 = X_{\dot{r}}u + Y_{\dot{r}}v + Z_{\dot{r}}w + K_{\dot{r}}p + M_{\dot{r}}q + N_{\dot{r}}r
\end{cases}
\tag{12}
$$

3.4. Viscous Hydrodynamic Damping Forces

Viscous resistance is a function of the velocity with respect to the current velocity. The relative velocity state vector of the ROV gives $x_r = [u_r, v_r, w_r, p, q, r]^T$, $x_r = x - x_c$, and $x_c = [u_c, v_c, w_c, 0, 0, 0]^T$, where x_c is the ocean current velocity. Moreover, the viscous resistance F_V can be written in a simplified form as follows:

$$
F_V = -Dx_r
\tag{13}
$$

where $D = D_L + D_Q$, $D_L x_r$ denotes the linear damping term, and $D_Q x_r$ represents the quadratic damping term. D_Q is very complex, and only its diagonal elements are kept as the influence of the coupling term is small. This is applicable to the modeling and simulation of a slow underwater vehicle. The hydrodynamic coefficients owing to the accelerations and angular accelerations of the vehicle can be obtained by using the planar motion mechanism model tests. D can be expressed as follows:

$$
D = - \begin{bmatrix}
X_u + X_{u|u|}|u_r| & X_v & X_w & X_p & X_q & X_r \\
Y_u & Y_v + Y_{v|v|}|v_r| & Y_w & Y_p & Y_q & Y_r \\
Z_u & Z_v & Z_w + Z_{w|w|}|w_r| & Z_p & Z_q & Z_r \\
K_u & K_v & K_w & K_p + K_{p|p|}|p| & K_q & K_r \\
M_u & M_v & M_w & M_p & M_q + M_{q|q|}|q| & M_r \\
N_u & N_v & N_w & N_p & N_q & N_r + N_{r|r|}|r|
\end{bmatrix}
\tag{14}
$$

3.5. Weight and Buoyancy

The gravity and the buoyancy of the ROV in the earth-fixed coordinate system give W and B, respectively. The gravity and the buoyancy in the body-fixed coordinates W_b, B_b can be obtained as follows:

$$
W_b = J_1^{-1} \begin{bmatrix} 0 \\ 0 \\ W \end{bmatrix}, B_b = -J_1^{-1} \begin{bmatrix} 0 \\ 0 \\ B \end{bmatrix}
\tag{15}
$$

Thus, the restoring force F_R has the following form:

$$
F_R = \begin{bmatrix} W_b + B_b \\ r_G \times W_b + r_B \times B_b \end{bmatrix}
\tag{16}
$$

The gravitational force and the buoyant force are defined in the global coordinate system, and therefore, they should be transformed to the local coordinate system as follows:

$$
F_R = -g = - \begin{bmatrix}
(W - B)\sin\theta \\
-(W - B)\cos\theta\sin\varphi \\
-(W - B)\cos\theta\cos\varphi \\
-(y_G W - y_B B)\cos\theta\cos\varphi + (z_G W - z_B B)\cos\theta\sin\varphi \\
(z_G W - z_B B)\sin\theta + (x_G W - x_B B)\cos\theta\cos\varphi \\
-(x_G W - x_B B)\cos\theta\sin\varphi - (y_G W - y_B B)\sin\theta
\end{bmatrix}
\tag{17}
$$

where $r_G = [x_G, y_G, z_G]^T$ and $r_B = [x_B, y_B, z_B]^T$ denote the locations of the gravitational and the buoyancy center of the ROV in the body-fixed frame, respectively.

3.6. Thruster Force and Moment

The ROV model considered in this study is equipped with seven thrusters. That is, T_1, T_2, T_3, and T_4 are installed horizontally and are responsible for the forward and sideward motions, while T_5, T_6, and T_7 are installed vertically at an inclined angle to induce the ascending and descending motions. The resultant forces and moments induced by all of the thrusters acting on the centroid in the body-fixed coordinate frame can be expressed as follows:

$$F_T = \begin{bmatrix} F_{Tx} & F_{Ty} & F_{Tz} & M_{Tx} & M_{Ty} & M_{Tz} \end{bmatrix}^T \tag{18}$$

where F_{Tx}, F_{Ty}, F_{Tz} are the three axial components of the resultant thrust force in the body-fixed coordinate system, and M_{Tx}, M_{Ty}, M_{Tz} are the three axial components of the resultant thrust moment.

3.7. Umbilical Cable Force

The umbilical cable plays an important role in facilitating the power supply and the communication function between the ROV and the support vessel. However, the attachment of the cable and the drag relative to the current places some restrictions on the maneuverability of the ROV. Therefore, the estimation of the corresponding effect caused by the umbilical cable and the current will be helpful for the controller design of the ROV. However, thus far, most of the researchers have neglected the effect of the umbilical cable because of the complexity involved, particularly in including the current effect.

There are two types of modeling techniques available to predict the response of tethered systems: continuous analytical methods and discrete numerical models [26]. Discrete numerical models are valid for some nonlinear properties such as the quadratic drag and the spatially varying properties of cables. The nonlinear coupling motion principle between the tether and the vehicle can be included in these models. The most prevalent numerical approaches used nowadays for determining the hydrodynamic performance of an underwater tethered system are the lumped mass method [27], the finite difference method [28,29], and the finite element method [30,31]. The lumped mass method is adopted in this study for cable simulation because of its simplicity and effectiveness [26].

In the present study, for simplifying the problem, the following assumptions are made to solve the configuration and tension of the umbilical cable attached to the ROV:

1. The umbilical cable is incompressible.
2. The cable surface is relatively smooth, ignoring the attachments on the cable.
3. The bending stiffness of the cable is ignored. The umbilical cable can only resist the tension force, but not the bending moment and the compression force.
4. The torsional rigidity and the quality of cable point rotation effect, which do not consider the torque, are ignored.

The umbilical cable force is one of the most important nonlinear disturbance forces on the ROV when the current is strong and the cable length is sufficiently long. The movement of a flexible cable moving in a fluid can be described by the following lumped parameter equations.

The cable model is described using the lumped parameters in the earth-fixed frame of O-XYZ. The coordinate system for analyzing the umbilical cable is shown in Figure 4. The origin O coincides with the end point of the umbilical cable. As shown in the figure, the cable is divided into n segments by ($n + 1$) nodes. The node number is sorted from the bottom to the top. The first node is on the ROV, and the last node is on the tether management system (TMS) or the surface ship. The jth segment refers to the segment between the jth node and the ($j + 1$)th node. Moreover, the segment is considered

a linear elastic unit with the same tension directing along the tangent of the segment as that shown in Figure 4.
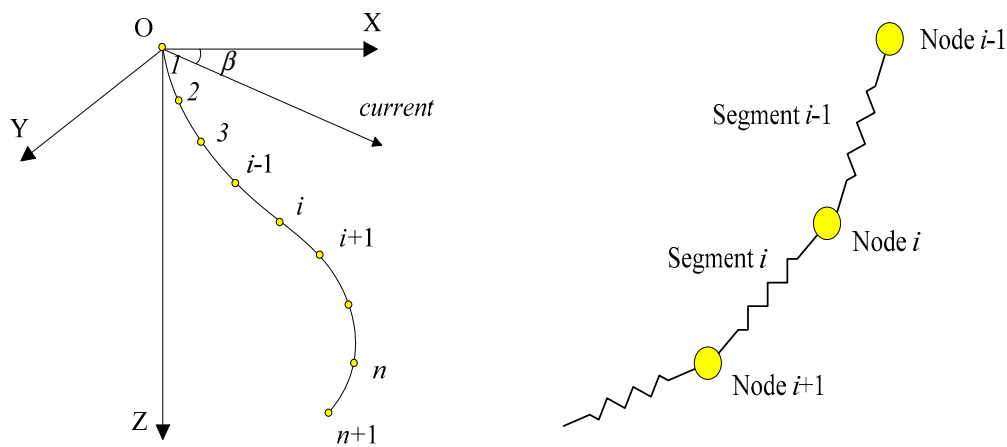
Figure 4. Discrete cable obtained using the lumped mass method.

According to the lumped mass model, the mass of each segment is distributed on the two boundary nodes equally and the nodes are connected with a light spring. Therefore, the first node bears half of the mass of the first segment as well as the last node in particular.

For the nodes except the first and the last, the kinetics equations of each node can be obtained by using Newton's laws of motion as follows:

$$m_i \frac{du_i}{dt} = W_i - B_i + F_{Ai} + D_i + T_i - T_{i-1} \tag{19}$$

$$\frac{dr_i}{dt} = u_i \tag{20}$$

where m_i is the ith lumped mass of the cable, u_i and r_i are the velocity and position vectors of the ith lumped mass with respect to the fixed inertial reference, and W_i and B_i are the gravity and buoyancy of the ith lumped mass. D_i represents the drag force, and T_i represents the tension force of the ith segment unit. F_{Ai} represents the additional mass force of the lumped mass with the following form:

$$F_{Ai} = m_a \left(\frac{du_c}{dt} - \frac{du_i}{dt} \right) \tag{21}$$

where m_a is the additional mass, $m_a = k_a \rho A l_0$, ρ is the sea water density, k_a is the additional mass coefficient, A is the cross-sectional area, l_0 is the initial segment length of the cable, and u_c is the current velocity.

As the cable shape is cylindrical, the drag force can be obtained according to the resistance formula of cylindrical objects in the current, and the resistance of each segment unit is distributed to the nodes at both the ends as follows:

$$D = -\frac{1}{2} \rho C S |v'| v' \tag{22}$$

where ρ is the sea water density; C is the cable resistance coefficient, which is often determined by tests; S is the incident flow area of the cylinder; and v' is the relative velocity to the flow. The drag force can be decomposed into the tangential and the normal components. The drag force lumped onto the ith node can be expressed as follows, and the hydrodynamic force on the umbilical cable can be resolved into the tangential component and the normal component.

$$D_{ti} = -\rho d_l C_t (|l_{i-1}| + |l_i|) |u_{ri} \tau_i| [(u_{ri} \tau_i) \tau_i] / 4 \tag{23}$$

$$D_{ni} = -\rho d_l C_n (|l_{i-1}| + |l_i|)|u_{ri} - (u_{ri}\tau_i)\tau_i|[u_{ri} - (u_{ri}\tau_i)\tau_i]/4 \tag{24}$$

where C_t, C_n are the tangential and the normal drag coefficients of the cable in the ith link, respectively, and l_i, u_{ri} can be calculated as follows:

$$l_i = r_{i+1} - r_i, \ (i = 1 \cdots n) \tag{25}$$

$$u_{ri} = u_i - u_c, \ (i = 2 \cdots n) \tag{26}$$

Thus, the lumped drag force on each node can be expressed as follows:

$$D_i = D_{ti} + D_{ni} \tag{27}$$

In fact, the cable is curved in the sea, and resistances at different points usually have different directions. To reduce the error due to the resistance direction, a tangential vector of average resistance is introduced. The unit tangential vector at the ith node is defined as follows:

$$\tau_i = (r_{i+1} - r_{i-1})/|r_{i+1} - r_{i-1}| \tag{28}$$

As the cable is equivalent to a discrete segmented spring model, the tension can be calculated according to Hooke's law when the tensile deformation of the spring unit occurs, as follows:

$$T = EA\varepsilon \tag{29}$$

where E denotes the elastic modulus of the piecewise cable unit, A is the cross-sectional area of the cable, and ε is the longitudinal strain. For an actual cable that can only be stretched, but not be compressed, the strain ε can only be positive. That is, there exists tension inside the cable when the segment unit is stretched more than the initial segmented length; otherwise, the tension is zero.

The tension force exerted in the ith link can be calculated by using the position of the nodes as follows:

$$T_i = \begin{cases} \pi d_i{}^2 E_i(|l_i| - l_0)l_i/(4l_0|l_i|), & |l_i| \geq l_0 \\ 0, & |l_i| < l_0 \end{cases} \tag{30}$$

3.8. Interaction Between the ROV and Umbilical Cable

When the ROV moves, it is pulled by the cable with tensile force. In turn, the movement of the ROV changes the position and the velocity of the end of the cable, thus changing the shape and the internal tension of the cable. The tension variation also affects the movement of the ROV and is a cyclic process. The interaction between the ROV and the umbilical cable can be described as follows:

$$u_{n+1} = J_1(v_1 + v_2 \times r_c) \tag{31}$$

$$r_{n+1} = r_{rov} + J_1 r_c \tag{32}$$

where J_1 is the transformation matrix and r_c is the position vector of the cable's tying point on the ROV in the body coordinate system.

For the ith node, u_i and r_i represent the displacement and the velocity, respectively. For the last node on the TMS or surface vessel without motion,

$$u_1 = u_s(t) \tag{33}$$

$$r_1 = r_s(t) \tag{34}$$

Because the cable is built on a fixed coordinate system, the tension is relative to the fixed system. The conversion matrix transformation is still required to calculate the ROV cable force in the O-xyz coordinate system as follows:

$$F_{bcable} = -J_1^{-1} T_{n+1} \tag{35}$$

$$M_{bcable} = r_c \times \left(-J_1^{-1} T_{n+1} \right) \tag{36}$$

Considering all of the abovementioned forces acting on the ROV, we can express the vector form of the dynamic model of the ROV in still water as follows:

$$M\dot{x} + C(x)x + D(x)x + g = F_T + F_{bcable} \tag{37}$$

where

$$\begin{cases} M = M_{RB} + M_A \\ C(x) = C_{RB}(x) + C_A(x) \end{cases} \tag{38}$$

$C(x)$ is the Coriolis and centripetal force matrix, $D(x)$ is the damping term, g is gravity and buoyancy, F_T is the control thrust, and F_{bcable} is the cable disturbing force in the body-fixed frame. When the existing currents, $\dot{x}_r = \dot{x} - \dot{x}_c$, $\dot{x}_c = 0$, are calculated using the relative velocity vector x_r to replace the ROV velocity x in the equations of motions, the general vector expressions for the dynamics equation of the ROV in the current can be expressed as follows:

$$M\dot{x}_r + C(x_r)x_r + D(x_r)x_r + g = F_T + F_{bcable} \tag{39}$$

where

$$\begin{cases} M = M_{RB} + M_A \\ C(x_r) = C_{RB}(x_r) + C_A(x_r) \end{cases} \tag{40}$$

4. Numerical Methods for the Solution

4.1. Numerical Integration Method

A set of coupled differential equations of the multi-body system can be solved simultaneously with dynamic equilibrium at each time step. The static equilibrium position of the system can be used to provide the initial condition. All of the nonlinearities (material, geometric, explicit loads, and hydrodynamic loads) are treated in a consistent manner. These governing equations are integrated by using the Runge–Kutta method.

4.2. Parameters and Calculation Steps

Because Equations (11) to (16) are a set of first-order ordinary differential equations with two-point boundary values, the Runge–Kutta method is applied to solve these equations. On the basis of the dynamic model of the ROV and the umbilical cable, the programming flow chart of cable simulation with the lumped parameter method is as follows (Figure 5):

For solving the nonlinear equations, an initial value must be given. In the previous studies, most researchers considered the straight line running steadily to be the initial configuration, and the vertical line of the cable in the still water was assumed as its initial state in this study. Further, the program allows running steadily in advance as the initial configuration.

An ROV with the principal dimensions of 3.17 m (length) × 1.81 m (beam) × 1.76 m (depth) is adopted as the numerical model for the calculations. The ROV is neutrally buoyant in the water. All the corresponding hydrodynamic coefficients of the maneuvering characteristics of the ROV can be obtained from previous work [32]. The connected point at the free surface near the supported vessel is assumed to be fixed at (0 m, 0 m, 0 m), and the other point of the cable connected to the ROV is set at

the gravitational center of the ROV. Parameters of the lumped parameter method for ROV simulation are shown in Table 2.
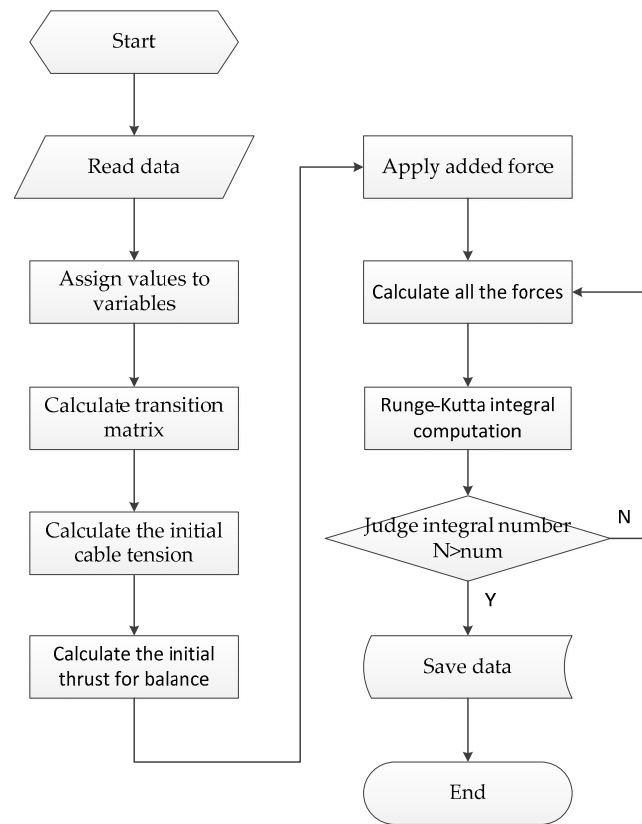
Figure 5. Flow chart of tethered ROV motion simulation.

Table 2. Parameters of the lumped parameter method (LPM).

Parameters	Values	Parameters	Values
Seawater density (kg/m^3)	1025	Cable length (m)	150
Drag coefficient in transverse direction C_n	1.2	Cross-sectional area (cm^2)	12.56
Drag coefficient in longitudinal direction C_t	0.024	Segment length (m)	15
Relative working depth (m)	100	Number of links	10
Diameter (m)	0.04	Segment mass (kg)	18.3
Young's modulus (N/m^2)	1.0×10^9	Mass in the water (kg/m)	0
Mass in the air (kg/m)	1.22	Minimum fracture strain (kN)	90

4.3. Comparison with Experiment

A small tank experiment is taken for comparison. The cable is fully immersed and allowed to reach the initial static configuration at the beginning. The experimental cable is initially suspended vertically and statically in the tank. The flow velocity is 1.543 m/s (3 kn), pulling a ball weighing 8.9 N in the water. The cable is 3.66 m long, and its diameter is 3.05 mm. The simulation time is 12 s.

The comparisons indicate that the simulated results are in fairly good agreement with the experiment (Figure 6). The slight discrepancy may be attributed to the inaccurate drag coefficients or certain non-modeled effects such as the bending stiffness of the cable.
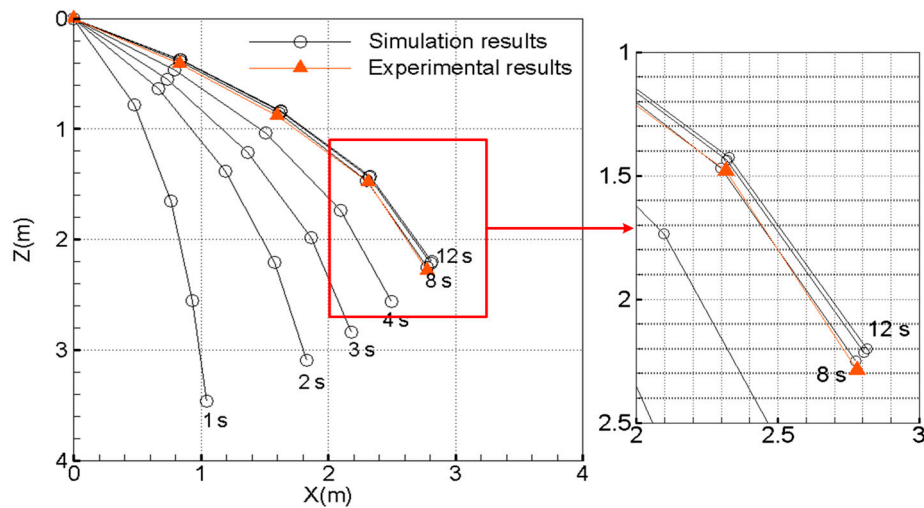
Figure 6. Comparison of the simulation results with the experimental results.

5. Nonlinear Observer

5.1. Nonlinear Observer Design

The ROV is a highly nonlinear and time-varying system with coupling between the degrees of freedom. For cases of weak maneuvering, the ROV's motion can be divided into horizontal and vertical motion, which can obtain satisfactory results. The control system of the ROV is often the integration of the multiple function modules, including the observer, controller units, and dead reckoning units.

Because the number of sensors that the ROV carries onboard is limited, only some of the state information can be measured. The nonlinear observer uses the measurable variables to estimate the velocities and the cable disturbing force information that cannot be measured online and in real-time. The structure diagram of the control system is shown below (Figure 7).
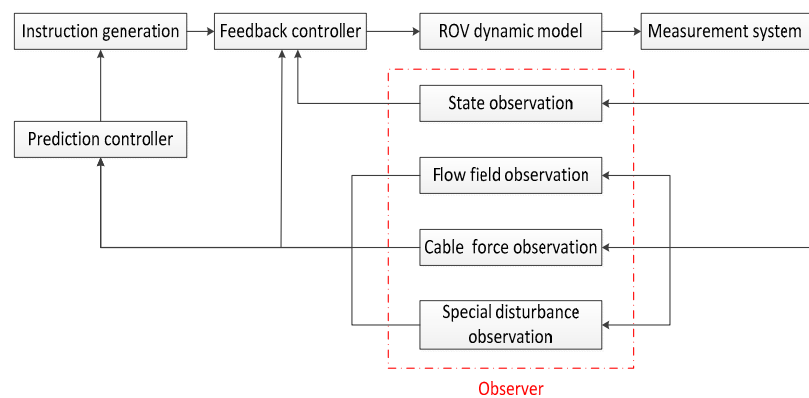
Figure 7. Control system structure of the ROV.

The observer structure (Figure 8) includes two parts: (1) The ROV dynamic model represents the dynamic and kinematic characteristics of the ROV in the water, including the ideal ROV model and the external disturbing cable force model, which is generated by using the lumped parameter method; (2) The observer model includes the ideal ROV model and a simplified model of the cable disturbing force.

The observer inputs are the thruster outputs $F_{Tx}, F_{Ty}, F_{Tz}, M_{Tz}$ in the body-fixed coordinates. The observer also needs measurements $u_{em}, v_{em}, w_{em}, r_{em}$ provided by the dead reckoning units. $\hat{u}, \hat{v}, \hat{w}, \hat{r}$ represent the observed values of u_e, v_e, w_e, r_e. e_u, e_v, e_w, e_r represent the observation

error. The observer outputs are the velocity estimation $\hat{u}_c, \hat{v}_c, \hat{w}_c$ and the cable disturbing force $F_{cablex}, F_{cabley}, F_{cablez}$.
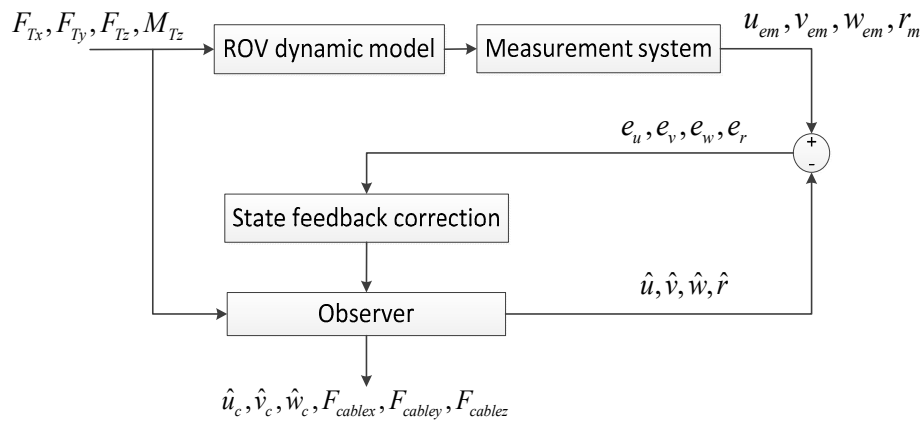
Figure 8. Observer structure.

Different types of sensors are installed on the ROV, such as the gyroscope, three-axis accelerometer, compass, Doppler velocity log, and the baseline system. Considering the equipment cost and the installation space, the number of sensors installed on ROV is limited. Some information cannot be obtained with sensors, such as the flow rate and the cable disturbing force. The nonlinear observer uses the measurable information to estimate the unknown state variables without any increase in the peripheral sensor equipment, and improves the overall performance of the system effectively.

An ROV always has a bilateral symmetrical structure, and its rolling and pitching motion velocities are small. Therefore, the influence of the rolling and pitching motion terms is often ignored. For the convenience of discussion, the ROV model can be simplified into a 4-DOF expression as follows:

$$\begin{cases} \dot{u}_r = \frac{1}{m-X_{\dot{u}}}\left[(m-Y_{\dot{v}})v_r r + X_u u_r + X_{u|u|}u_r|u_r| + (F_{Tx}+F_{bcablex})\right] \\ \dot{v}_r = \frac{1}{m-Y_{\dot{v}}}\left[-(m-X_{\dot{u}})u_r r + Y_v v_r + Y_{v|v|}v_r|v_r| + \left(F_{Ty}+F_{bcabley}\right)\right] \\ \dot{w}_r = \frac{1}{m-Z_{\dot{w}}}\left[Z_w w_r + Z_{w|w|}|w_r|w_r + (W-B+F_{Tz}+F_{bcablez})\right] \\ \dot{r} = \frac{1}{I_{zz}-N_{\dot{r}}}\left[(Y_{\dot{v}}-X_{\dot{u}})u_r v_r + N_r r + N_{r|r|}r|r| + (M_{Tz}+M_{bcablez})\right] \end{cases} \tag{41}$$

The motion function can be written as follows:

$$\begin{cases} \dot{X} = u_r\cos\psi - v_r\sin\psi + u_c \\ \dot{Y} = u_r\sin\psi + v_r\cos\psi + v_c \\ \dot{Z} = w_r + w_c \\ \dot{\psi} = r \end{cases} \tag{42}$$

The current model can be expressed as follows:

$$\begin{cases} \dot{u}_c = -\mu_{cx}u_c + \omega_{cx} \\ \dot{v}_c = -\mu_{cx}v_c + \omega_{cy} \\ \dot{w}_c = -\mu_{cx}w_c + \omega_{cz} \end{cases} \tag{43}$$

where $\mu_{cx}, \mu_{cy}, \mu_{cz} > 0, \omega_{cx}, \omega_{cy}, \omega_{cz}$ are the white noise with a mean value of zero. (41)–(43) express the 4-DOF model. Next, a reasonable state observer is designed to observe the unmeasurable parameters with sensors such as u_c, v_c, w_c.

For linear systems, the observer theory is almost complete and mature. Research on the nonlinear system state observer began in the 1970s, and various types of nonlinear observers have been developed

and applied to different fields since then. In 1974, Utkin proposed a sliding mode observer using a switch function, which is often used in sliding mode control [33]. Its advantage is that when the nonlinear term and the disturbance of the system are bounded, it exhibits good robustness. This observer has invariance for the disturbance and uncertain factors when the matching conditions are satisfied. In view of the above advantages, sliding mode observers have been widely used and studied.

As the exact mathematical model of an ROV is difficult to build and will be affected by the external disturbance, the sliding mode observer is considerably suitable for such a system. Therefore, (41)–(43) can be rewritten as follows:

$$\begin{cases} \dot{\chi} = f(\chi) + BF_T + B\sigma \\ \eta = J\chi \end{cases} \tag{44}$$

The observation function is as follows:

$$y = \eta - \omega \tag{45}$$

where ω represents the measurement noise. $\chi = [u_r, v_r, w_r, r, u_c, v_c, w_c]^T$, $\eta = [\dot{X}, \dot{Y}, \dot{Z}, \dot{\psi}]^T$, F_T represents the control input, and σ represents the sum of the model error and the external disturbance. Further, σ is assumed to be bounded, that is, $\|\sigma\| \leq \beta_1$.

A nonlinear observer is designed as follows:

$$\begin{cases} \dot{\hat{\chi}} = f(\hat{\chi}) + BF_T + L\tilde{y} + \Gamma \\ \hat{\eta} = J\hat{\chi} \\ \hat{y} = \hat{\eta} \end{cases} \tag{46}$$

where $\tilde{y} = y - \hat{y}$, $\Gamma = \rho \text{sgn}(\tilde{y})$ is the switching compensation term, $\rho \geq \beta_1$. The switching compensation term is used to represent the effects of the system modeling error and the external disturbance to enhance the robustness of the observer.

Taking (44) and (45) minus (46), and $e = \chi - \hat{\chi}$, $\tilde{\eta} = \eta - \hat{\eta}$, we obtain the following error functions:

$$\begin{cases} \dot{e} = f(\chi) - f(\hat{\chi}) + B\sigma - L\tilde{y} - \Gamma \\ \tilde{\eta} = Je \\ \tilde{y} = \tilde{\eta} - \omega = Je - \omega \end{cases} \tag{47}$$

Then:

$$\dot{e} = f(\chi) - f(\hat{\chi}) + B\sigma - LJe + L\omega - \Gamma \tag{48}$$

Let $\|L\omega\| \leq \beta_2$, as $e \approx 0$; then, $f(\chi) - f(\hat{\chi})$ can be expressed as follows:

$$f(\chi) - f(\hat{\chi}) = Ae + \Delta(e) \tag{49}$$

where Ae represents the linear part and $\Delta(e)$ represents the nonlinear part. Assuming $\|\Delta(e)\| \leq \beta_3$ and substituting (49) into (48) yields the following equation:

$$\begin{aligned} \dot{e} &= Ae + \Delta(e) + B\sigma - LJe - \Gamma + L\omega \\ &= (A - LJ)e - \Gamma + \Delta(e) + B\sigma + L\omega \\ &= A_0 e - \Gamma + \Delta(e) + B\sigma + \omega_1 \end{aligned} \tag{50}$$

where $\omega_1 = L\omega$, $A_0 = A - LJ$, and (50) is the differential equation of the observed error.

The following assumptions are put forward:

(1) If (A, J) is observable, then there exists L making A_0 stable.

(2)　There exists a positive definite symmetric matrix P and a positive definite matrix Q, satisfying Lyapunov's equation as follows:

$$A_0^T P + PA_0 = -Q \tag{51}$$

The stability of the nonlinear observer as shown in (49) is proven as follows:
Let Lyapunov's function $V(e) = e^T Pe$; then,

$$
\begin{aligned}
\dot{V} &= \dot{e}^T Pe + e^T P\dot{e} \\
&= (A_0 e - \Gamma + \Delta(e) + B\sigma + \omega_1)^T Pe + e^T P(A_0 e - \Gamma + \Delta(e) + B\sigma + \omega_1) \\
&= e^T(A_0^T P + PA_0)e + 2e^T P(\Delta(e) + B\sigma + \omega_1 - \Gamma) \\
&= -e^T Qe + 2e^T P(\Delta(e) + B\sigma + \omega_1 - \rho\mathrm{sgn}(\widetilde{y}))
\end{aligned} \tag{52}
$$

Let $\lambda_{\min}(Q)$ and $\lambda_{\max}(P)$ be the minimum characteristic root of Q and the maximum characteristic root of P, respectively; then,

$$\dot{V} \leq -\lambda_{\min}(Q)\|e\|^2 + 2\|e\|\lambda_{\max}(P)(\beta_1 + \beta_2 + \beta_3 + \rho) \tag{53}$$

As $\dot{V} \leq 0$ and $\|e\| \geq 0$,

$$\|e\| \geq R_e \tag{54}$$

where $R_e = 2\frac{\lambda_{\max}(P)}{\lambda_{\min}(Q)}(\beta_1 + \beta_2 + \beta_3 + \rho)$. Therefore, when (54) exists, the observer is stable and the observation error decreases gradually until it enters the spherical domain with a radius of R_e centered on the origin in an n-dimensional space. After entering the spherical domain, the state estimation error reduces to a certain degree and oscillates, meeting the following condition:

$$\|e\| \leq R_e \tag{55}$$

From (55), we infer that the observer error is uniformly bounded. To reduce the observer error, when given P, Q, β_2, β_3, an effective method is to model the disturbing force and the disturbance compensation to reduce β_1. Even though the disturbance model cannot fully represent the actual disturbance, it can effectively reduce the upper bound of the observation error and considerably weaken the chatter of the observer.

5.2. Cable Disturbance Force Simplified Model

To improve the precision of the observer, there are usually two methods. One is to improve the structure of the observer and design an optimization algorithm and an adaptive method to improve the robustness of the observer. The advantage of this method is that the algorithm robustness for the parameter perturbation can be proven in theory for a particular system. However, its limitation is that it is difficult to find a universal observer satisfying the requirements of different systems.

The other method is to model the unknown disturbing force. Modeling the disturbing force can reflect the main factors of the disturbing force and make the feedforward compensation for the observer, thus reducing the upper bound of the unknown disturbance force and improving the precision of the observation. The advantage of this approach is that it is applicable to any observer for performance improvement.

The observer state variables are $\chi = [u_r, v_r, w_r, r, u_c, v_c]^T$, and the observer formula can be expressed as follows:

$$
\begin{cases}
\dot{\hat{\chi}} = f(\hat{\chi}) + B(F_T + J^{-1}F_{cable}(\hat{\chi})) + L\widetilde{y} + \Gamma \\
\hat{\eta} = C\hat{\chi} \\
\hat{y} = \hat{\eta}
\end{cases} \tag{56}
$$

6. Results and Discussion

6.1. Simulation of Cable Disturbing Force

The spatial changing rule of the cable disturbing force is analyzed and discussed, and a simplified model of the cable disturbing force is attempted for use in the design of the observer to reduce the influence of the cable disturbing force on the observer.

In the numerical calculation model, the cable disturbing force is calculated using the lumped mass method iteratively and is regarded as the true value of the cable force in a real circumstance. A simplified model of the cable disturbing force also needs to be built for the observer as the disturbing compensation. The cable disturbing force is generated by the relative motion of the cable in the water and is influenced by various parameters, such as the current velocity, displacement and velocity boundary conditions of the cable ends, cable length, and the cable material properties.

The simulation results are given below for different operating conditions, and the simplified model structure of the cable disturbing force is discussed.

Case one: The top end and the bottom end of cable are static at the initial time; the top end coordinates of the cable are (0 m, 0 m, 0 m), and the bottom end coordinates of the cable are (0 m, 0 m, 100 m). Further, the current velocity is (u_c, 0 m/s, 0 m/s). Tension results under different conditions of cable length and working depth are shown in Table 3.

Table 3. Tension on the ROV at the end of the cable under different conditions.

Cable Length (m)	Working Depth (m)	u_c (m/s)	F_{cablex} (N)	F_{cabley} (N)	F_{cablez} (N)
120	100	0	0	0	0
		−0.25	−55.45	0	−45.58
		−0.3	−79.44	0	−68.01
		−0.5	−220.21	0	−190.68
		−0.75	−495.29	0	−428.54
		−1	−880.45	0	−761.07
		−1.25	−1375.20	0	−1186.70
		−1.5	−1979.45	0	−1704.94
150	100	0	0	0	0
		−0.25	−44.96	0	−19.66
		−0.5	−179.66	0	−82.12
		−0.75	−404.16	0	−184.76
		−1	−719.00	0	−329.74
		−1.25	−1123.27	0	−514.93
		−1.5	−1617.16	0	−740.76
150	125	0	0	0	0
		−0.25	−68.47	0	−58.53
		−0.5	−275.12	0	−237.54
		−0.75	−619.05	0	−535.34
		−1	−1100.30	0	−950.30
		−1.25	−1718.30	0	−1480.80
		−1.5	−2472.94	0	−2125.86

Case two: The top end of the cable is static with the coordinates (0 m, 0 m, 0 m), and the bottom end of the cable moves with the absolute velocity (u, 0 m/s, 0 m/s); the relative current velocity is (u_r, 0 m/s, 0 m/s), and the current velocity is (u_c, 0 m/s, 0 m/s). Tension results under different relative velocity conditions are shown in Table 4.

Table 4. Tension on the ROV under different relative velocity conditions.

Cable Length (m)	Working Depth (m)	u_c (m/s)	u_r (m/s)	u (m/s)	F_{cablex} (N)	F_{cablez} (N)
		−1.5	1.5	0	−1617	−741
		−1.5	1.6	0.1	−1731	−790
150	100	−1.5	1.8	0.3	−1970	−895
		−1.5	2	0.5	−2230	−1000
		−1.5	2.2	0.7	−2500	−1125
		−1.5	2.4	0.9	−2800	−1250

It can be seen that when the top end of the cable is static and the bottom end moves, the tension components F_{cablex} and F_{cablez} at the end of the cable on the ROV have a linear relationship with the relative velocity with respect to the current, and have the opposite direction of the relative velocity.

To conclude, the tension at the end of the cable on the ROV is a complex function of the relative velocity to the current, displacement, and velocity boundary conditions of the cable ends, the cable length, and so on. When the cable length is 150 m and the top end of the cable is static, the expressions of the cable terminal tension versus the relative velocity and the spatial position under the typical velocity conditions can be expressed as follows.

When the current velocity is (−1.5 m/s, 0 m/s, 0 m/s), the top end of the cable is static with the coordinates (0 m, 0 m, 0 m) and the bottom end of the cable or the ROV moves. The ROV often swims against the current in the water, and the lateral and vertical velocities are relative small. Therefore, the effect of the longitudinal velocity on the cable tension is mainly considered here. The tension components at the bottom end of the cable to the ROV can be expressed as follows:

$$F_{cablex} = 366 - 1308u_{re} + \left[-0.3381X - 0.0164Y^2 - 0.025(Z - 100)^2 - 3.1634(Z - 100) \right] \times 9$$

$$F_{cabley} = -0.9126Y \times 9$$

$$F_{cablez} = 114 - 564u_{re} + \left[-0.0076X^2 + 0.5277X - 0.0125Y^2 - 0.077(Z - 100)^2 - 3.6955(Z - 100) \right] \times 9 \tag{57}$$

where u_{re} is the relative current velocity component along the x direction in earth coordinates, $u_{re} = u_e - u_c$. Further, u_e is the absolute velocity in earth coordinates and u_c is the current velocity. Equation (57) is mainly used for estimating the disturbance compensation in the observer.

The tension components at the end of the cable F_{cablex}, F_{cablex}, F_{cablez} are obtained in the earth coordinate system. The cable tension in the body-fixed coordinate system of the ROV can be obtained with a coordinate transformation.

6.2. Observer Simulation under Ideal Condition without Cable Disturbing Force

The state variables adopt $q = [u_r, v_r, w_r, r, u_c, v_c]^T$, the observer variables adopt $\eta = [\dot{X}, \dot{Y}, \dot{Z}, \dot{\psi}]^T$, and the observer parameters adopt $L = diag\{5, 5, 5, 5, 5\}$, $\rho = diag\{0.5, 0.5, 0.5, 5, 5\}$. When there is no cable disturbing force, σ is zero in (44). The parameters of the slowly varying current flow field model are $\mu_{cx} = 1$, $\mu_{cy} = 1$. ω_{cx} and ω_{cy} are composed of the Gaussian white noise signal and the step signal. The amplitudes of the step signals are −0.4 and −0.3, respectively, and the power spectrum density of the white noise is 10^{-5}. The current velocity generated by (43) is regarded as the true value of the current velocity, and the current velocity averages (−0.4 m/s, −0.3 m/s, 0 m/s). The effects of the measurement noise are ignored, and the propeller thrust acting on the ROV is $F_T = (2000N, 500N, 0N)$. The simulation time is 100 s, and the simulation step size is 0.001 s.

From the above figures, we can infer that if the effect of the sensor noise is not considered, when the system model does not have the current velocity and the cable disturbing force, the observer can rapidly track the observation state variables, including the ROV's position, attitude angle, velocity, and current velocity (Figures 9–11). The tracking error is small, as the velocity observation error is less than 0.02 m/s, and the displacement observation error is less than 0.03 m (Figure 12). This shows that the designed state observer has good observation performance without divergence in the ideal circumstance.

6.3. Observer Simulation under Conditions of Cable Disturbing Force without Compensation

To observe the effects of the cable disturbing force on the performance of the observer, the cable force is considered in the ideal ROV model. The cable disturbing force mentioned above is generated by using the lumped parameter method, regarded as the true value in practical environments. The parameters adopted by the lumped parameter method are presented in Table 2. The observer simulation is conducted under the conditions of a cable disturbing force without the disturbance compensation and depends only on the observer's own robustness. The parameters of the observer remain unchanged. The effects of the measurement noise are ignored. The current velocity averages $(-0.5 \text{ m/s}, 0 \text{ m/s}, 0 \text{ m/s})$, and the propeller thrust acting on the ROV is $F_T = (2000N, 0N, 0N)$. The simulation time is 50 s, and the simulation step size is 0.001 s. The simulation results are presented below.

As can be seen from the observation results, the observation errors of the current velocity and the relative velocity of the ROV increase obviously (Figure 13). Although the observer has certain robustness, the added cable disturbing force (Figure 14) affects the accuracy of the observation (Figures 15 and 16). Therefore, when there exist external disturbances in the model or the actual system, the external disturbance has a considerable influence on the observation accuracy, and part of the observation information may possibly exhibit a divergence trend.
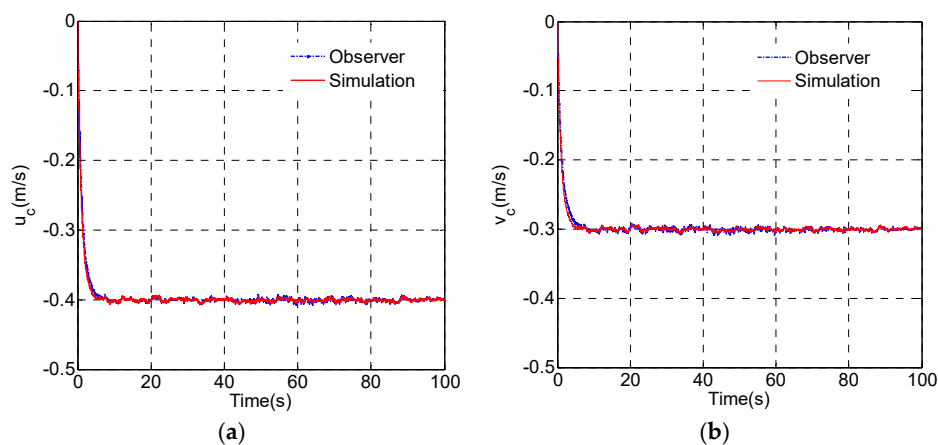
Figure 9. Observed results of current velocity: (**a**) current velocity in the X direction of earth-fixed frame; (**b**) current velocity in the Y direction of earth-fixed frame.
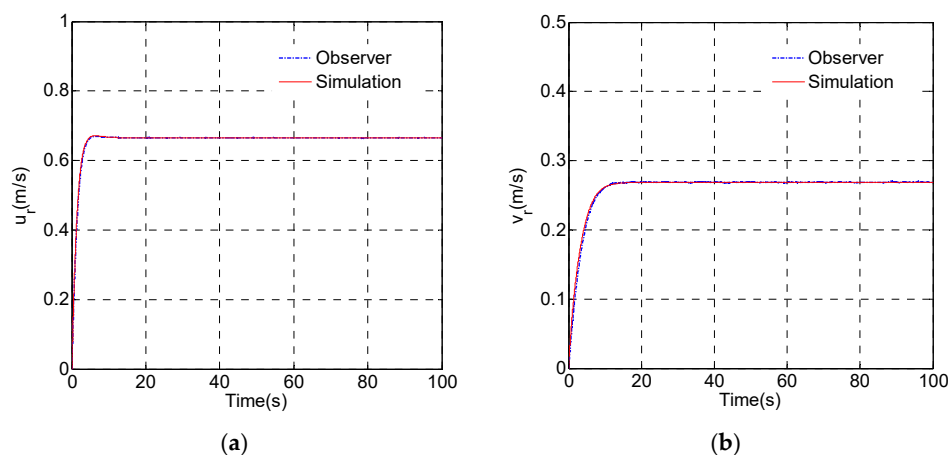
Figure 10. Observed results of relative velocity: (**a**) relative velocity of ROV in the x direction of body-fixed frame; (**b**) relative velocity of the ROV in the y direction of body-fixed frame.
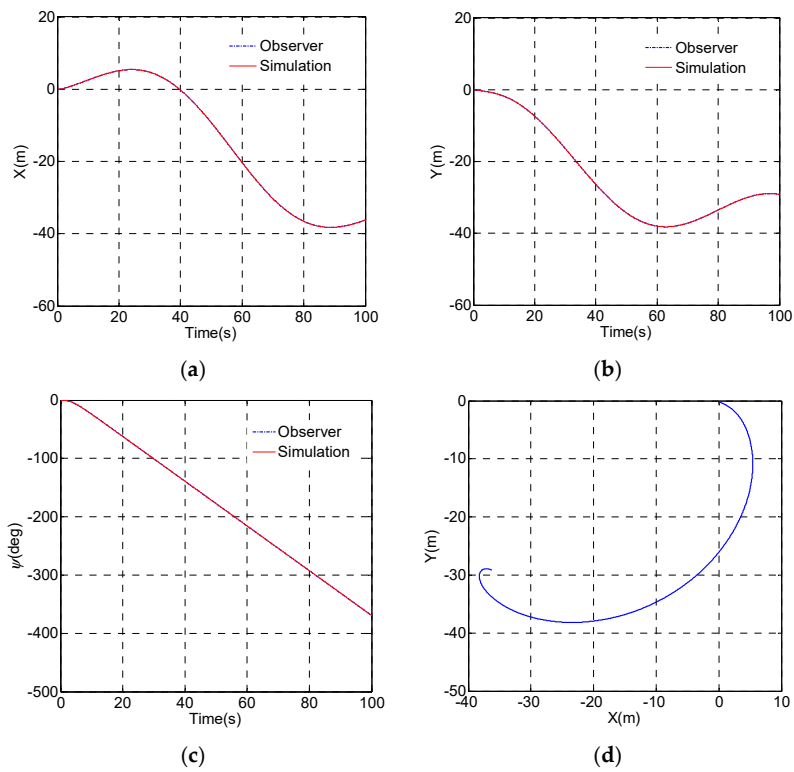
Figure 11. Observed results of position and heading of ROV: (**a**) X; (**b**) Y; (**c**) heading; (**d**) trajectory of ROV in the XY plane.
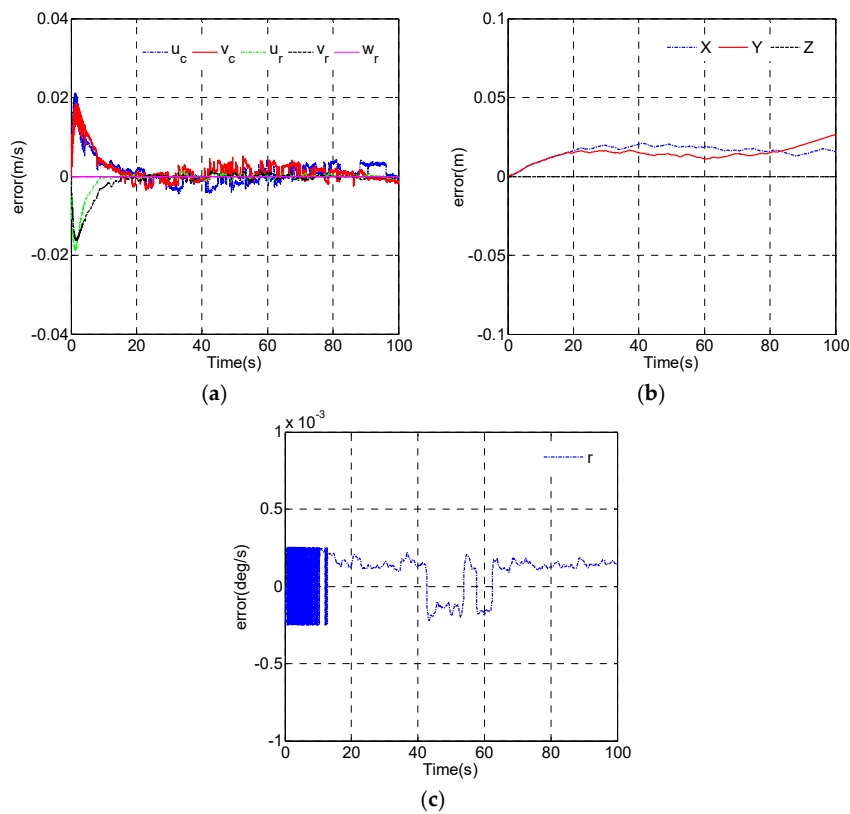
Figure 12. Observed errors of velocity and position: (**a**) velocity error; (**b**) position error; (**c**) angular velocity error.
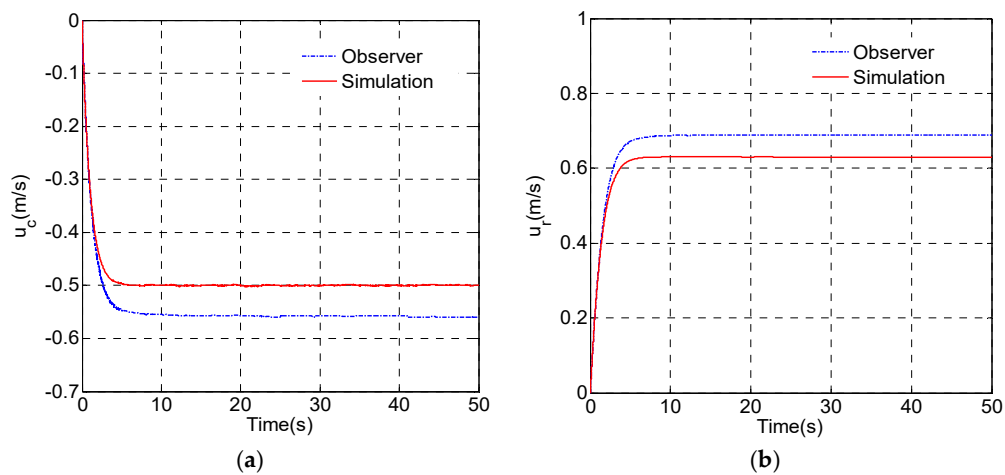
Figure 13. Observed result of velocity: (**a**) current velocity in the X direction; (**b**) relative velocity of ROV in the x direction.
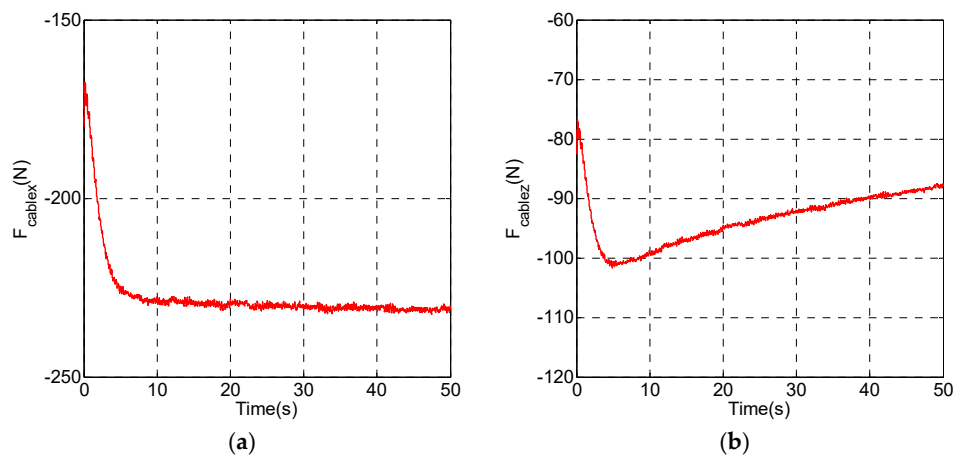
Figure 14. Cable disturbing force (LPM): (**a**) cable force in the X direction; (**b**) cable force in the Z direction.
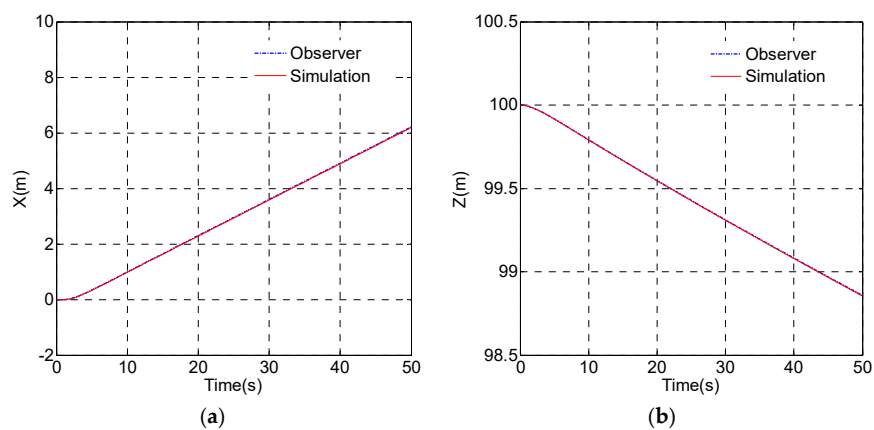
Figure 15. Observed result of ROV position: (**a**) X; (**b**) Z.
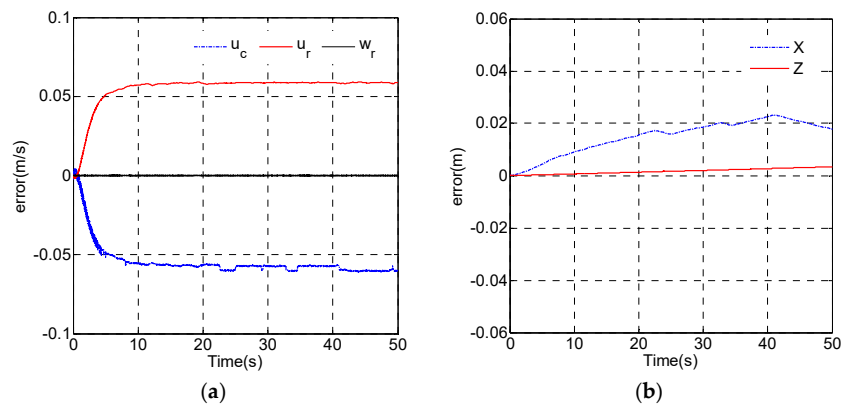
Figure 16. Observed error of velocity and position: (**a**) velocity error; (**b**) position error.

6.4. Observer Simulation under Conditions of Cable Disturbing Force with Compensation

To observe the effects of the cable disturbing force compensation on the performance of the observer, the cable force is considered in the ideal ROV model. The cable disturbing force mentioned above is generated by using the lumped parameter method, regarded as the true value in practical environments. The initial cable shape in the vertical plane is shown in Figure 17. The observer simulation is conducted under the conditions of a cable disturbing force with disturbance compensation. The parameters of the observer remain unchanged, $L = diag\{5, 5, 5, 5, 5\}$, $\rho = diag\{0.5, 0.5, 0.5, 5, 5\}$. The effects of the measurement noise are ignored. The current velocity averages (-0.5 m/s, 0 m/s, 0 m/s). The simulation time is 100 s, and the simulation step size is 0.001 s.
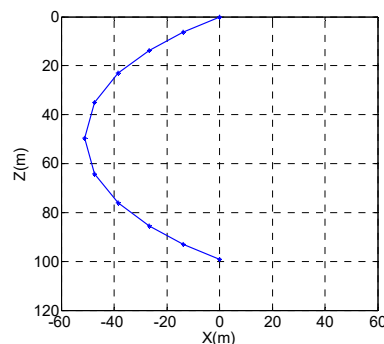
Figure 17. Initial cable shape in the vertical plane.

When the propeller thrust acting on the ROV is $F_T = (2000N, 0N, 0N)$, the following simulation results are obtained.

The simulation results show that when the longitudinal thrust acts on the ROV system, the observation accuracy of state variables u_r, w_r, u_c is improved considerably by the addition of the cable disturbing force compensation to the observer model compared with the observations without compensation (Figures 18 and 19). The absolute value of the velocity observation error decreases from 0.05 m/s to 0.01 m/s, and the vertical displacement observation error becomes 0.12 m after 100 s (Figure 20), which is acceptable. The cable disturbing force error between the observed value and the true value is small, and the observed result can accurately reflect the variation in the disturbance force (Figure 21).
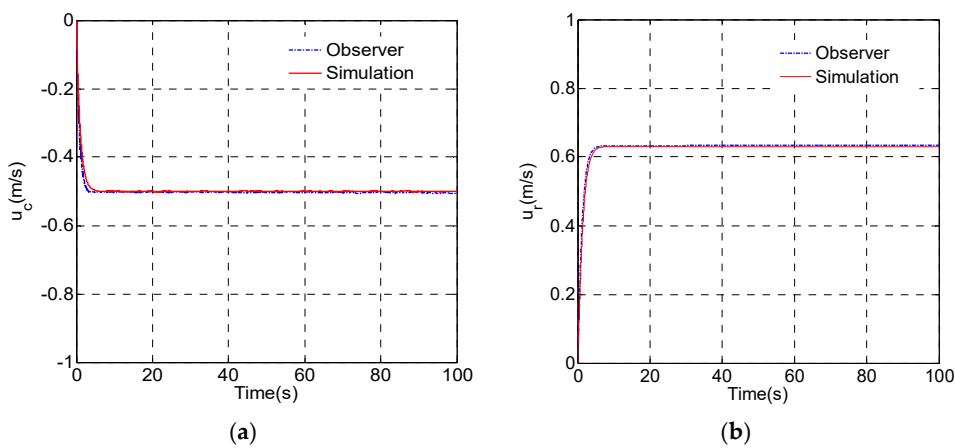
Figure 18. Observed result of velocity: (**a**) current velocity in the X direction; (**b**) relative velocity of ROV in the x direction.
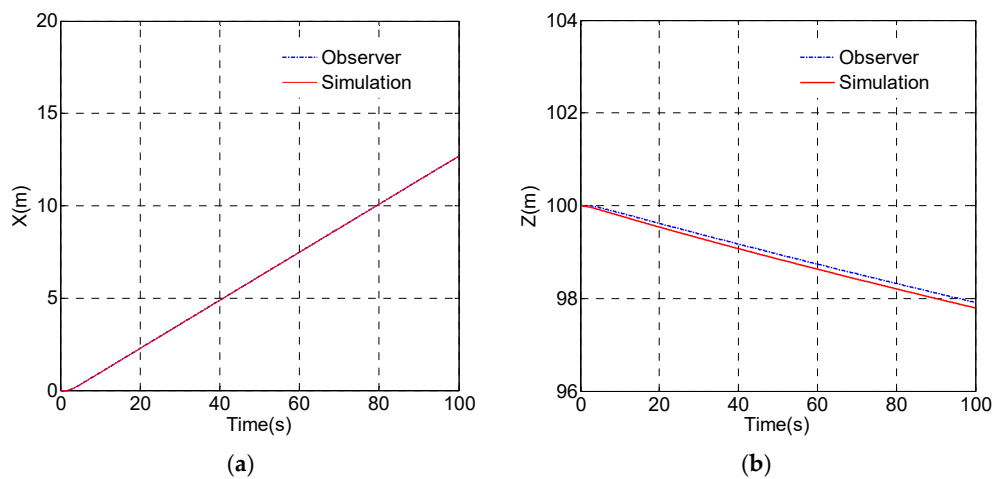
Figure 19. Observed result of ROV position: (**a**) position in the X direction; (**b**) position in the Z direction.
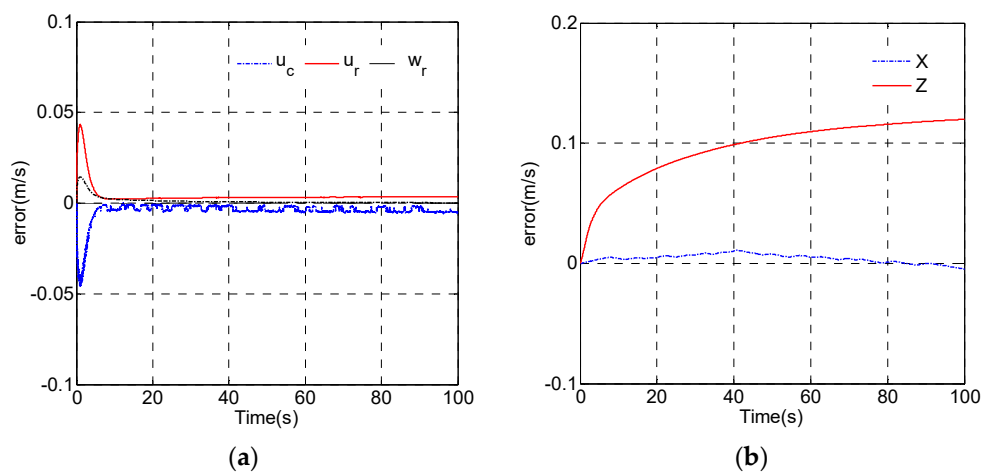
Figure 20. Observed error of velocity and position: (**a**) velocity error; (**b**) position error.
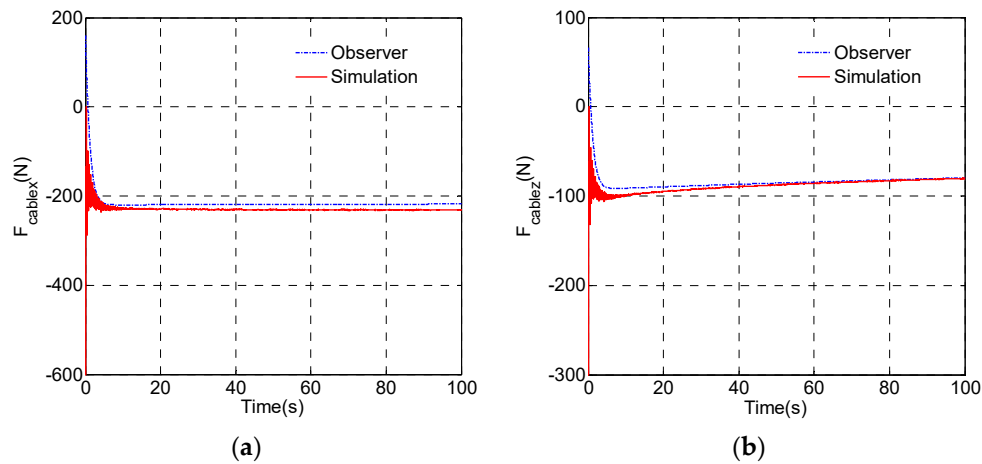
Figure 21. Cable disturbing force (LPM): (**a**) cable force in the X direction; (**b**) cable force in the Z direction.

It is concluded that as the existence of the disturbing force deteriorates the observer performance, modeling the disturbance force and compensating for the observer is an effective method to increase the accuracy of the observer without modifying its parameters, although disturbing force modeling cannot fully characterize the cable disturbing force.

When the ROV's resultant thrust is $F_T = (3000N, 0N, 0N)$, the simulation results are as follows.

When the ROV's vertical thrust increases from 2000 N to 3000 N, the observation results of the state variables u_r, w_r, u_c are still effective and have a high observation precision (Figures 22 and 23). The absolute value of the velocity observation error converges within 0.01 m/s (Figure 24). The vertical displacement observation error is relatively large, mainly because the vertical component error between the observed value and the true value of the cable disturbing force is relatively large, of which the relative error is around 10% (Figure 25). It is illustrated that the established simplified model of the cable disturbing force can accurately reflect the change in the disturbing force at different velocities, which is effective and universal.
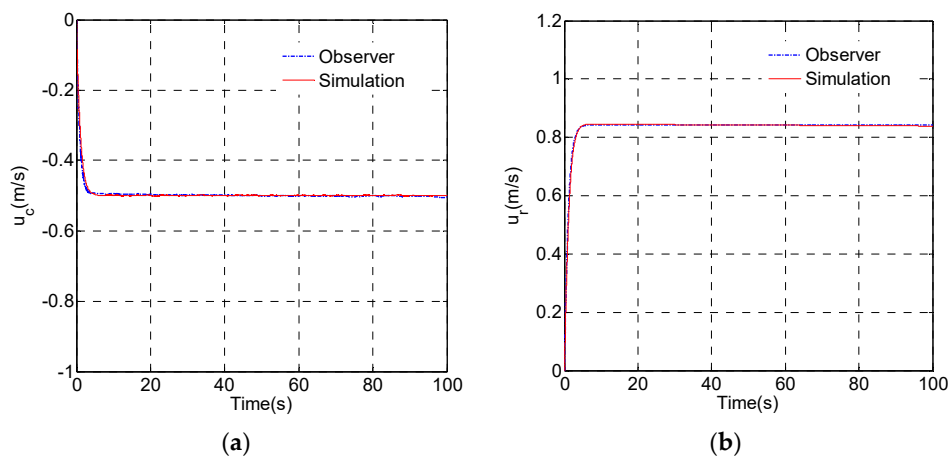
Figure 22. Observed result of velocity: (**a**) current velocity in the X direction; (**b**) relative velocity of ROV in the x direction.
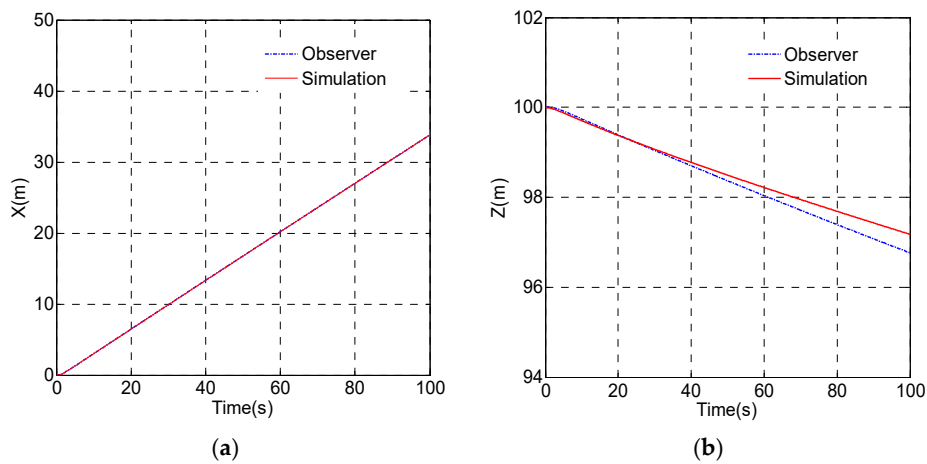
Figure 23. Observed result of ROV position: (**a**) position in the X direction; (**b**) position in the Z direction.
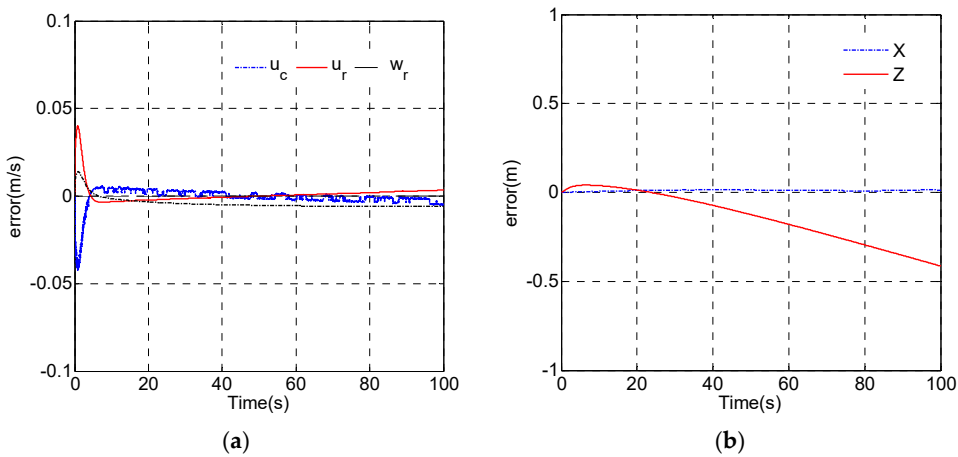
Figure 24. Observed error of velocity and position: (**a**) velocity error; (**b**) position error.
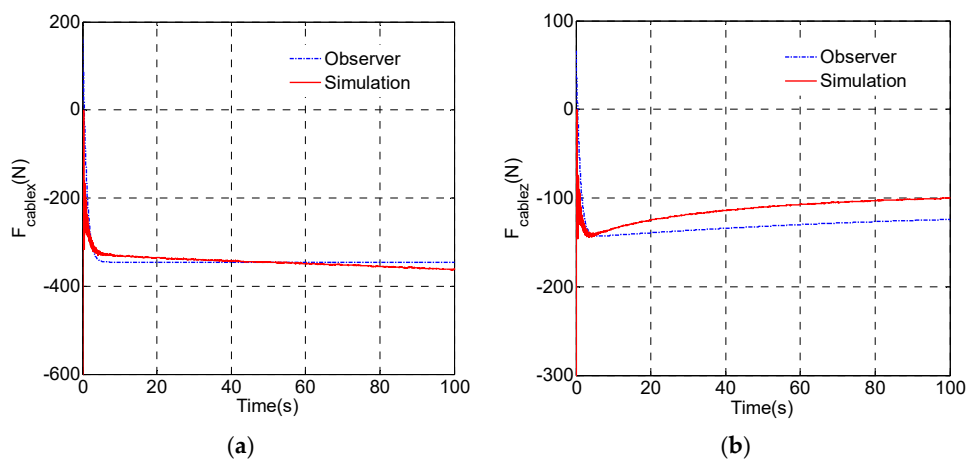
Figure 25. Cable disturbing force: (**a**) cable force in the X direction; (**b**) cable force in the Z direction.

7. Conclusions

A nonlinear observer for the ROV was investigated, and a 4-DOF nonlinear sliding state observer was designed in this study. A 6-DOF dynamic model was set up under the condition of ocean current.

The lumped mass method was adopted for the dynamic simulation of the umbilical cable and verified by a comparison with the experimental data. A coupling dynamic model of the ROV and the umbilical cable was established. Further, a 4-DOF nonlinear sliding mode observer for the ROV system was set up, and the ocean current model and the simplified flexible cable disturbance force model were established. The convergence and the stability of the observer were proven, and the applicability and the performance of the observer were verified by simulation under different working conditions. Unmeasured states such as the velocity state, current velocity, and cable disturbance were observed with the designed observers. We concluded that establishing a simplified disturbance model that could effectively estimate the actual disturbing force, and adopting the disturbing force compensation method effectively improved the observation precision and reduced the chattering of the observer outputs; doing so can also provide a basis and a reference for the design and application of other tethered ROV systems.

Author Contributions: X.L. designed the disturbance estimator and the integration with the main observer, and wrote the manuscript. M.Z. conceived and designed the nonlinear observer. T.G. analyzed the results and wrote the manuscript.

Conflicts of Interest: The authors declare that there is no conflict of interest.

References

1. Do, K.D.; Pan, J. *Control of Ships and Underwater Vehicles: Design for Underactuated and Nonlinear Marine Systems*; Springer: Berlin, Germany, 2009.
2. Cohan, S. Trends in ROV development. *Mar. Technol. Soc. J.* **2008**, *42*, 38–43. [CrossRef]
3. Yoerger, D.; Slotine, J. Robust trajectory control of underwater vehicles. *IEEE J. Ocean Eng.* **1985**, *10*, 462–470. [CrossRef]
4. Bessa, W.M.; Dutra, M.S.; Kreuzer, E. Depth control of remotely operated underwater vehicles using an adaptive fuzzy sliding mode controller. *Robot. Auton. Syst.* **2008**, *56*, 670–677. [CrossRef]
5. Bagheri, A.; Moghaddam, J.J. Simulation and tracking control based on neural-network strategy and sliding-mode control for underwater remotely operated vehicle. *Neurocomputing* **2009**, *72*, 1934–1950. [CrossRef]
6. Cui, R.; Zhang, X.; Cui, D. Adaptive sliding-mode attitude control for autonomous underwater vehicles with input nonlinearities. *Ocean Eng.* **2016**, *123*, 45–54. [CrossRef]
7. Soylu, S.; Proctor, A.A.; Podhorodeski, R.P.; Bradley, C.; Buckham, B.J. Precise trajectory control for an inspection class ROV. *Ocean Eng.* **2016**, *111*, 508–523. [CrossRef]
8. Cui, R.; Chen, L.; Yang, C.; Chen, M. Extended state observer-based integral sliding mode control for an underwater robot with unknown disturbances and uncertain nonlinearities. *IEEE Trans. Ind. Electron.* **2017**, *64*, 6785–6795. [CrossRef]
9. Wang, Y.; Gu, L.; Gao, M.; Zhu, K. Multivariable output feedback adaptive terminal sliding mode control for underwater vehicles. *Asian J. Control* **2016**, *18*, 247–265. [CrossRef]
10. Kinsey, J.C.; Whitcomb, L.L. Model-based nonlinear observers for underwater vehicle navigation: Theory and preliminary experiments. In Proceedings of the IEEE International Conference on Robotics and Automation, Roma, Italy, 10–14 April 2007; pp. 4251–4256.
11. Song, B.K.; An, J.H.; Choi, S.B. A New Fuzzy Sliding Mode Controller with a Disturbance Estimator for Robust Vibration Control of a Semi-Active Vehicle Suspension System. *Appl. Sci.* **2017**, *7*, 1053. [CrossRef]
12. Fernandes, D.D.A.; Sørensen, A.J.; Pettersen, K.Y.; Donha, D.C. Output feedback motion control system for observation class ROVs based on a high-gain state observer: Theoretical and experimental results. *Control Eng. Pract.* **2015**, *39*, 90–102. [CrossRef]
13. Gauthier, J.P.; Kupka, I.A.K. Observability and observers for nonlinear systems. *SIAM J. Control Optim.* **1994**, *32*, 975–994. [CrossRef]

14. Fridman, L.; Shtessel, Y.; Edwards, C.; Yan, X.G. Higher-order sliding-mode observer for state estimation and input reconstruction in nonlinear systems. *Int. J. Robust Nonlin. Control* **2008**, *18*, 399–412. [CrossRef]

15. Rezazadegan, F.; Shojaee, K.; Chatraei, A. Design of an adaptive nonlinear controller for an autonomous underwater vehicle. *Int. J. Adv. Electr. Electron. Eng.* **2013**, *2*, 1–8.

16. Khadhraoui, A.; Beji, L.; Otmane, S.; Abichou, A. Observer-based controller design for remotely operated vehicle ROV. In Proceedings of the IEEE International Conference on Informatics in Control, Automation and Robotics, Vienna, Austria, 1–3 September 2014; pp. 200–207.

17. Chu, Z.; Zhu, D.; Jan, G.E. Observer-based adaptive neural network control for a class of remotely operated vehicles. *Ocean Eng.* **2016**, *127*, 82–89. [CrossRef]

18. Kinsey, J.C.; Eustice, R.M.; Whitcomb, L.L. A survey of underwater vehicle navigation: Recent advances and new challenges. In Proceedings of the IFAC Conference of Manoeuvering and Control of Marine Craft, Lisbon, Portugal, 20–22 September 2006.

19. Refsnes, J.E.; Pettersen, K.Y.; Sorensen, A.J. Control of slender body underactuated AUVs with current estimation. In Proceedings of the 45th IEEE Conference on Decision and Control, San Diego, CA, USA, 13–15 December 2006; pp. 43–50.

20. Aguiar, A.P.; Pascoal, A.M. Dynamic positioning and way-point tracking of underactuated AUVs in the presence of ocean currents. *Int. J. Control* **2007**, *80*, 1092–1108. [CrossRef]

21. Børhaug, E.; Pivano, L.; Pettersen, K.Y.; Johansen, T.A. A model-based ocean current observer for 6DOF underwater vehicles. *IFAC Proc.* **2007**, *40*, 169–174. [CrossRef]

22. Lueck, R.G.; Driscoll, F.R.; Nahon, M. A wavelet for predicting the time-domain response of vertically tethered systems. *Ocean Eng.* **2000**, *27*, 1441–1453. [CrossRef]

23. Fang, M.C.; Chen, J.H.; Luo, J.H.; Hou, C.S. On the behavior of an underwater remotely operated vehicle in a uniform current. *Mar. Technol.* **2008**, *45*, 241–249.

24. Zhu, K.Q.; Zheng, D.C.; Cai, Y.; Yu, C.L.; Wang, R.; Liu, Y.L.; Zhang, F. Nonlinear hydrodynamic response of marine cable-body system under random dynamic excitations. *J. Hydrodyn. Ser. B* **2009**, *21*, 851–855. [CrossRef]

25. Fossen, T.I. *Guidance and Control of Ocean. Vehicles*; John Wiley & Sons: Chichester, UK, 1994.

26. Driscoll, F.R.; Lueck, R.G.; Nahon, M. Development and validation of a lumped-mass dynamics model of a deep-sea ROV system. *Appl. Ocean Res.* **2000**, *22*, 169–182. [CrossRef]

27. Walton, T.S.; Polachek, H. Calculation of transient motion of submerged cables. *Math. Comput.* **1960**, *14*, 27–46. [CrossRef]

28. Sanders, J.V. A three dimensional dynamic analysis of a towed system. *Ocean Eng.* **1982**, *9*, 483–499. [CrossRef]

29. Ablow, C.M.; Schechter, S. Numerical simulation of undersea cable dynamics. *Ocean Eng.* **1983**, *10*, 443–457. [CrossRef]

30. Leonard, J.W. Nonlinear dynamics of cables with low initial tension. *J. Eng. Mech.* **1972**, *98*, 293–309.

31. Ma, D.C.C.; Chu, K.H.; Leonard, J.W. Slack-elasto-plastic dynamics of cable system. *J. Eng. Mech. Div.* **1979**, *105*, 207–222.

32. Xu, G.; Ge, T.; Zhu, J.M.; Lian, L. Motion modelling and simulation of varying length cable for "Sea Dragon 3500" ROV. *Mar. Technol.* **2005**, *5*, 22–26. (In Chinese)

33. Utkin, V.I. Sliding mode and their application in discontinuous systems. *Automat. Rem. Control* **1974**, *1*, 1898–1907.